Journal of Fluorescence (2019) 29:231–240
https://doi.org/10.1007/s10895-018-2332-2

ORIGINAL ARTICLE

Ligand-Induced Conformational Changes near the Active Site Regulating Enzyme Activity of Momorcharins from Seeds of Bitter Gourd

Chie Matsunaga[1] · Yuuki Okada[1] · Etsuko Nishimoto[1]

Received: 5 November 2018 / Accepted: 10 December 2018 / Published online: 19 December 2018

Abstract
It is reasonable to consider that Type I-ribosomal inactivation proteins (RIP) retain some specific affinity to harmful pathogens to complete the role as a bio-defense relating protein. In the present studies, it was shown that two Type I-RIPs, α- and β-momorcharins, maintained the abilities to bind with N-acetylglucosamine (NAG) to change the conformation around the active sites and to regulate their N-glycosidase activities. By the binding of NAG, the freedom of internal motion of Trp192 in α-momorcharin was increased 1.5 times near the active site and, on the other hand, the corresponding motion of Trp190 was limited 50% in β-momorcharin. The results in the fluorescence resonance excitation energy transfer experiments demonstrated that Trp-190 of β-momorcharin was kept away from Tyr-70 but Trp192 contrarily approached closer to the nearest neighboring Tyr residue consisting of the active center of α-momorcharin by the binding with NAG. These conformational changes near the active site close correlated with promotion and/or suppression of the N-glucosidase activities of β- and α-momorcharins.

Keywords N-glycosidase · Ribosome-inactivating protein (RIP) · Fluorescence anisotropy · FRET · TCSPC

Introduction

Many plants secrete a variety of bio-defense relating materials to conserve the own species against attacks from virus, bacteria, algae and other harmful pathogens. Ribosome-inactivating proteins (RIP) included in seeds, leaves or roots of almost every Dicotyledonare complete the bio-defensive actions in every stage in growth [1–5]. While over 100 species of RIPs were identified after the first recognition, the first confirmation of the enzymatic function of RIPs as N-glycosidase was comparatively recent. Endo et al. pointed out that RIPs removed single adenine residue from a specific sequence (GAGA) in a universally conserved loop at the top of the stem in 28 S rRNA, so called sarcin/ricin domain [6]. But now, it is well known that the substrate specificity of RIPs is not so strict and RIPs display the N-glycosidase activity against many kinds of RNA, even against DNA [7–12]. Because of such adenine releasing reaction, RIPs inactivate the peptide elongation reaction in protein synthesis process on the ribosome of harmful pathogens.

Momorcharins are included in seeds of bitter gourd and both of α- and β-momorcharin are known to be constituted of single peptide chain similarly to Pokeweed anti-viral protein (PAP) in *Phytolacca ammericana* and Trichosanthin in *Trochosanthes kirilowii*. According to X-ray structure, momorcharin is consisted of two domains, one is N-terminal and the other C-terminal domains. Their sequences stretch from the N-terminal to Ileu179 and from Ser180 to the C-terminal, respectively. N-terminal domain includes two sub-domains to keep the whole structure stable as the back born structure and to give constituting peptide unit some flexibility, respectively. The former is compactly assembled α-helices and the latter is constituted in stacked β-structures. On the other hand, C-terminal domain is constructed with loosely packed β-structures and α-helices. As shown in Fig. 1, the active site of momorcharin which is consisted of two Tyrs, Glu and Arg is arranged at the adjacent part of N-and C-terminal domains. Two tyrosine residues (Tyr70, Tyr111 of α-momorcharin, Tyr70, Tyr109 of β-momorcharin) clamp ribose moiety of RNA and Arginine and Glutamic acid residues (Arg163, Glu160 of α-momorcharin, Arg161, Glu187 of β-momorcharin) catalyze the adenine-releasing reaction in cooperation with each other at the respective active center [13].

✉ Etsuko Nishimoto
enish@brs.kyushu-u.ac.jp

[1] Laboratory of Biophysical Chemistry, Faculty of Agriculture, Graduate School of Kyushu University, 744 Motooka, Nishi-ku, Fukuoka 819-0395, Japan

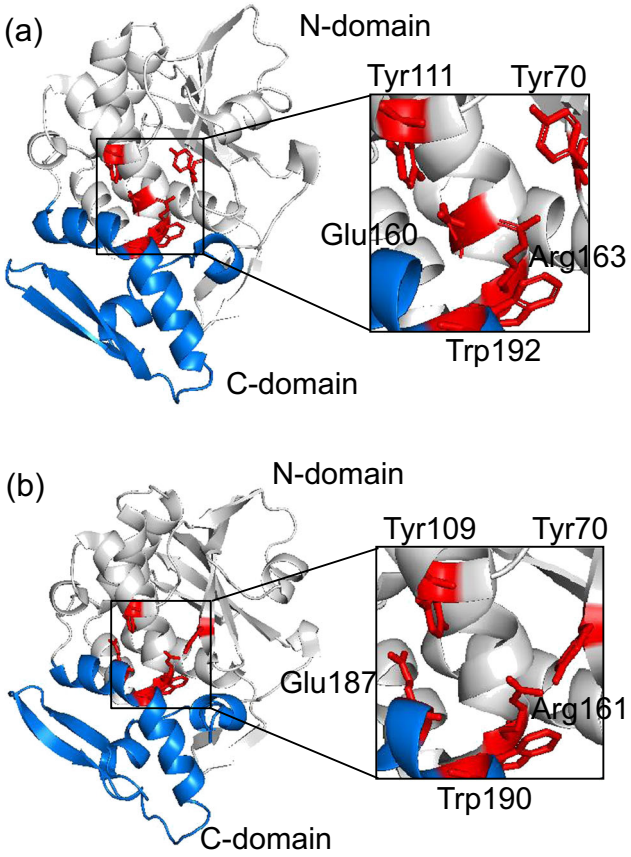

Fig. 1 X-ray crystal structure of α-momorcharin (**a**) and β-momorcharin (**b**). The partial structures of the active center were extended in the insertions. Amino acids consisting of the active center were indicated by three letters code. The N-terminal and C-terminal domains are indicated by light gray and blue, respectively. The structures of α-momorcharin and β-momorcharin were based on PDB code 3N1N and 1CF5, respectively

The most interesting and advantageous characteristics in the structures of momorcharins and also in other RIPs is that single Trp residue (W192 of α-momorcharin, W190 of β-momorcharin) locates at the lid part of the active center. Valuable information on the structural stability and correlations between the conformation and protein function have been reported through the unique fluorescence spectroscopic properties of Trp residue. The fluorescence spectral sift indicates the change in the hydrophobicity due to the packing of amino acid residues around Trp residue [14]. The fluorescence lifetime and decay kinetics well reveal the interactions of Trp residue with the surrounding amino acid residues [15]. The distance and mutual orientation between Trp and Tyr are reflected in the resonance excitation energy transfer to substantiate the alteration of the active center of the enzyme [16] and the rotational correlation times and motional freedoms of Trp residue measured by the steady state and time-resolved fluorescence anisotropy would give the information on the approaching and deleting contact of substrate with binding site [17, 18]. As reported by Fukunaga, these entities are essential for elucidating the relationships between the conformation and enzymatic activity in momorcharins [19].

RIPs are classified into three types according to their constitutions. Type II and Type III of RIP additionally equip the sugar binding sub-units (B chain) in addition to the polypeptide chain with N-glycosidase activity (A chain) to enhance the affinity and efficiency of biodefense activity against various pathogens [20]. Type I RIP is consisted of a single polypeptide and no apparent functional domain is recognized. However, it would be reasonable to assume that Type I RIPs also ubiquitously preserve affinity to some component of cell wall and membrane of bacteria and other pathogen. Indeed, the binding of N-acetylglucosamine (NAG) was reported in the functional analysis studies of two α- and β-momorcharin [21, 22]. Furthermore, Nakashima et al. proposed that Pokeweed antiviral protein (PAP) which belongs to Type I RIPs exhibited affinities to N-acetylglucosamine (NAG) and other sugars to modify the enzymatic activity [23]. The regulation mechanism of enzymatic activity of RIPs has to be clearly solved to understand the physiological role of RIPs, because RIPs are considered to be suicide proteins and keep a possibility to inhibit the own protein synthesis on the ribosome in plant cells similarly to in the external harmful pathogens. In order to sustain the own cells sound, many plants must establish some regulation mechanism of the activity of RIPs. From this point of view and to make good use of RIPs, studies on ligand binding effect on the enzymatic activity and structures would be significant as the first step to clear up the regulation mechanism of RIPs activity. Recently, RIPs are started to be used as the medical treatments against some tumors and cancers and as the controlling agent for HIV [24].

In the present studies, we show that two Type I-RIPs, momorcharins (α- and β-momorcharin) potentially retain the ability to bind with N-acetylglucosamine (NAG). Furthermore, it is also shown that the subtle conformational changes are induced near the active site to adjust the enzymatic activity by the binding of N-acetylglucosamine.

Materials and Methods

Materials

Seeds of bitter gourd (*Momordica charantia*) were purchased from Nakahara Co. Ltd. (Fukuoka, Japan). N-acetylglucosamine (NAG) and other reagents for constituting buffer systems were obtained from Sigma (St. Louis, MO, USA). Mono-S and DEAE-Sepharose used for ion-exchange chromatography were purchased from GE Healthcare Bio-Science Corp (Piscataway, NJ, USA). Other chemicals were of analytical grade and used without further purification.

Isolation and Purification of Momorcharins

Isolation and purification methods of α- and β-momorcharins were based on Fong et al. [25]. Crude enzymes were extracted to the buffer solution (2 mM sodium phosphate buffer, pH 7.5) from the grinded powders of seeds of bitter gourd (*Momordica charantia*) which was defatted in advance. The precipitation in the saturated ammonium sulfate solution was re-suspended in the 2 mM of phosphate buffer and dialyzed against the 2 mM of phosphate buffer overnight at 4 °C. The condensation of enzyme was conducted with the anion-exchange chromatographing using HiPrep DEAE column. The non-adsorbed fraction against the anion-exchange column was collected and adopted to the cation-exchange chromatography (Mono-S column). Two N-glucosidases, α- and β-momorcharins were obtained as the fractions of 50 mM and 65 mM of NaCl, respectively. The purifications of α- and β-momorcharins were confirmed by observing the single band with 29 kDa in the SDS-PAGE.

Enzymatic Activity

The activities of α- and β-momorcharins were evaluated by measuring precisely the trace of enzymatically isolated adenine from RNA. The enzymatic reaction mixtures were adjusted by adding 100 μL of baker's yeast RNA (1.0 mg/mL) and 50 μL of buffer solution to the 100 μL of momorcharin solution of which concentration was adjusted constant ($OD_{280} = 0.05$) in spectroscopic method. The NAG effects on the enzymatic reaction were examined by resolving 50 mM NAG in the 50 μL buffer solutions. The enzymatic reaction was stopped by adding 20 μL of 3 M/L of sodium acetate and 200 μL of 100% ethanol. Completing the ethanol precipitation, the reaction mixture was incubated for 15 min. at −80 °C and removed the enzymatic product except adenine by centrifugation at 12,000×g for 15 min. The supernatant fluid including adenine was condensed under vacuum in the desiccator. The quantitative analysis of adenine released by enzymatic reaction of momorcharin was performed using a HPLC (JASCO, type 807-IT) with YMC-Pac ODS-AQ column and uv-absorption system at 260 nm. In order to improve the precision for the quantitative analysis of enzymatically released adenine, two kinds of references were adopted, one included non-enzyme, the other was measured in the conditions that the enzymatic reaction time was substantially zero.

Steady-State Fluorescence

The steady-state fluorescence spectrum of momorcharins was measured using fluorescence spectrophotometer FP-8200 (JASCO). The excitation wavelength was set at 295 nm to excite exclusively Trp in momorcharins.

The fluorescence spectra were strictly corrected against the detection and excitation system. The undesired stray light was removed by subtraction procedures.

In the studies on the NAG-binding with momorcharins, NAG was dissolved in 2 mM of sodium phosphate buffer to reach to 1 mM and them small aliquots of NAG solution was added to the buffer solutions including 1.59 μM of α-momorcharin or 0.75 μM of β-momorcharin. After the incubation for 10 min to complete the equilibrium, the fluorescence spectrum was measured with pay attentions to the differences induced by NAG.

Time-Resolved Fluorescence Intensity and Anisotropy Decays

Time-resolved fluorescence intensity and anisotropy decays measurements were performed using the apparatus with the subpicosecond laser based time-correlated single photon counting system (TCSPC) [26]. The excitation pulse was generated from the combination of femtosecond Ti:Sapphire laser (TSUNAMI, Spectra-physics, Mountain View, CA), pulse picker (model 3980, Spectra-physics), and third harmonic generator (GWU, Spectra-physics). The repetition rate was 800 kHz and the full-width at half-maximum (FWHM) of excitation pulse was 100 fs. The stop pulse to drive the time-to-amplitude converter (TAC, Ortec, Oak Ridge, TN) was obtained by a high speed avaranche photodiode (APD, C5658, Hamamatsu Photonics, Shizuoka, Japan). The fluorescence emission pulse was detected by a multichannel plate type photomultiplier (3809 U-50, Hamamatsu photonics) with high speed amplifier (C5594, Hamamatsu photonics) and amplified by fast timing amplifier (FTA, 820, Ortec) to employ as the start pulse for TAC. The start and stop pulses were fed into TAC through constant fraction discriminators (CFD, 935, Ortec). The output signals from TAC were accumulated in 2048 channels in multichannel analyzer (Maestro-32, Ortec). The channel width was 8.6 ps/ch. The FWHM of instrumental response function was 150 ps.

The fluorescence decay kinetics were described with a linear combination of exponentials,

$$F(t) = \sum \alpha_i \exp(-t/\tau_i) \quad (1)$$

Where, $F(t)$ was the time-resolved fluorescence, τ_i was the fluorescence decay time of i-th component and α_i was the corresponding pre-exponential factor. The decay parameters, α_i and τ_i were determined by iterative convolution and non-linear curve fitting method. Adequacy of curve fitting was judged by the residual plots, the serial variance ratio (SVR) and sigma value [27].

In time-resolved fluorescence anisotropy decay measurements, a Gran-Tayor polarizer was set just behind the sample to measure the decays of vertical ($I_{VV}(t)$) and horizontal ($I_{VH}(t)$) emission against the vertical excitation. These two

polarized fluorescence were connected with the fluorescence intensity decay, $F(t)$ and anisotropy decay, $r(t)$, through the equation, Eq. (2) and Eq. (3).

$$I_{VV}(t) = \frac{1}{3}F(t)\{1 + 2r(t)\} \quad (2)$$

$$I_{VH}(t) = \frac{1}{3}F(t)\{1 - r(t)\} \quad (3)$$

The fluorescence anisotropy decay kinetics was given by Eq. (4).

$$r(t) = \sum_i \beta_i \exp(-t/\varphi_i) \quad (4)$$

Where, ϕ_i and β_i were the rotational correlation time of i-th component and the corresponding amplitude, respectively. The decay parameters of $F(t)$ and $r(t)$ were simultaneously determined by the global analysis in non-linear curve-fitting using Eqs. (2) and (3). The adequacies of their decay parameters were confirmed by SVR and sigma value for the decays of $I_{VV}(t)$ and $I_{VH}(t)$.

Results and Discussion

Binding of Momorcharins with NAG

The fluorescence spectra of α- and β-momorcharin showed a maximum at 330 nm to show that the circumstance surrounding the Trp residue was hydrophobic near the active site. The fluorescence intensity was decreased by addition of N-acetylglucosamine without any changes in spectral line shape and maximum wavelength. The induced change in the fluorescence intensity was not so large, but it reached to the constant value after the reductions responding to the added concentration of NAG as shown in the insert of Fig. 2.

These results demonstrate that the decrease in the fluorescence is due to the binding of momorcharins with NAG. The decrease in the fluorescence intensity was plotted based on Hill equation [23].

$$\Delta F = \frac{\Delta F^{max} \cdot C^k}{K_d^k + C^k} \quad (5)$$

Where, K_d was the dissociation constant, C, the concentration of NAG, ΔF^{max}, maximum value in the induced fluorescence change by the binding of NAG, and k, Hill index to indicate the co-operativity of NAG binding with momorcharin.

As shown in Fig. 3a, b, binding properties of momorcharins with NAG were characterized with two experimental parameters, K_d and k determined by such the way that the momorcharin-NAG titration curve give the best fits against Hill Eq. (5). The binding parameters of momorcharin with NAG were summarized in Table 1.

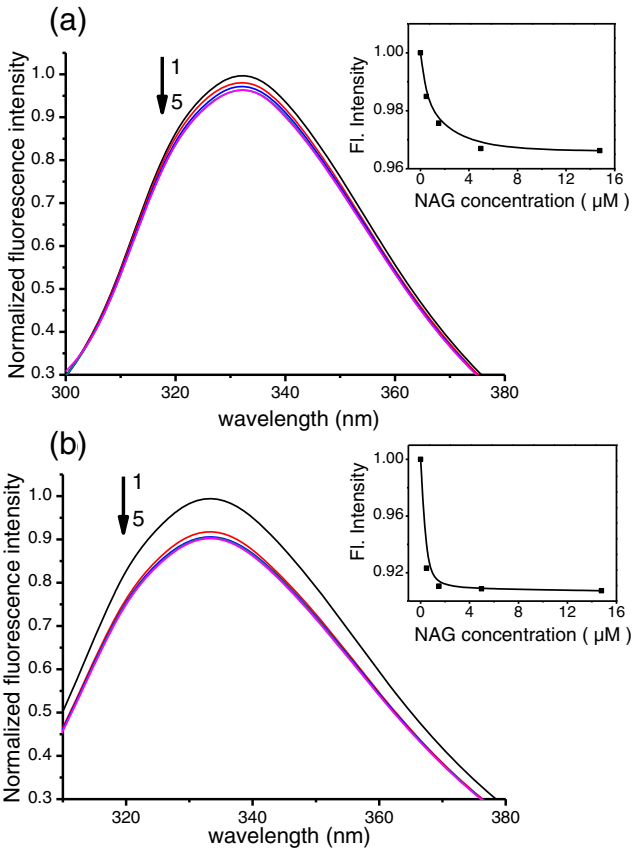

Fig. 2 NAG effect on the fluorescence spectra of α-momorcharin (**a**) and β-momorcharin (**b**). The excitation wavelength was 295 nm. The slit for Ex/Em was 5 nm/5 nm. Concentrations of α-momorcharin (**a**) and β-momorcharin (**b**) were 1.59 μM and 0.75 μM, respectively. The spectra of 1, 2, 3, 4 and 5 were measured in the presence of 0, 0.48, 1.50, 4.98 and 14.78 μM of NAG, respectively. The change in the fluorescence intensity at the maximum wavelength was shown in the insertions

The dissociation constant of α- and β-momorcharins were 0.700 μM/L and 0.054 μM/L, respectively to show that β-momorcharin retains the higher affinity to NAG than α-momorcharins. The co-operativity index of β-momorcharin was 0.47 to suggest that two binding sites of momorcharin exclusively bound NAG each other. The binding of NAG to one binding site of β-momorcharin would suppress the binding with the other site. The number of binding site (n) per single molecule of momorcharin was given by the relation, $n = [NAG]^s / [momorcharin]$. $[NAG]^s$ is the concentration of NAG where every binding sites of momorcharin reach to the saturation under the conditions that the induced fluorescence change is linearly increased with the added NAG. The linear lines obtained under the low concentration region of NAG reached to the maximum at the NAG concentration giving the molecular ratio, $n = [NAG]^s / [momorcharin] = 2$. This result suggests that both of two momorcharins equip two binding sites against NAG although the positions of the binding sites are not specified in the present studies. Gajraj et al. showed in their functional analysis based on the X-ray

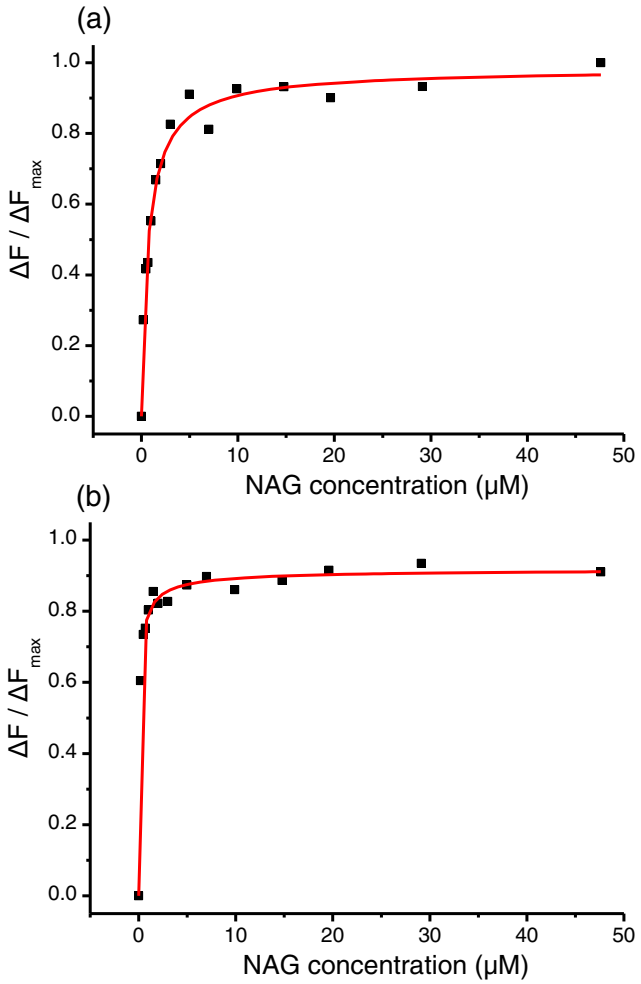

Fig. 3 Hill plots of the induced fluorescence intensity change of α-momorcharin (**a**) and β-momorcharin (**b**) against the concentrations of NAG. The plots were based on the Hill equation, $\frac{\Delta F}{\Delta F_{max}} = \frac{c^k}{K_d^k + c^k}$, where ΔF, induced fluorescence change; ΔF_{max}, maximum value of ΔF; K_d, the dissociation constant; c, concentration of NAG and k, Hill coefficient for the binding of momorcharin with NAG. The concentration of α-momorcharin and β-momorcharin were 1.59 μM and 0.75 μM, respectively

structure that two NAG molecules adjacently bound with Pro11, Asn227, Thr229 and Ser30 of α-momorcharin [21]. Furthermore, it was reported that Asp1, Asn3, Asn51 and Thr53 similarly participated in the binding of β-momorcharin with NAG [22]. Their propositions are quite consistent with our results although the binding site of momorcharins could not be specified in the present case.

Table 1 Binding parameters of momorcharins with NAG

	K_d (μM)	k	n
α-MMC	0.700	0.92	2
β-MMC	0.054	0.47	2

MMC, momorcharin; K_d, Dissociation constant; k, Hill coefficient; n, Number of bining site

Segmental Rotation of Trp Residue near the Active Site

The changes in the conformation and molecular dynamics around the active site close correlate with the enzymatic activity. The segmental rotation of Trp192 (α-momorcharin) and Trp190 (β-momorcharin) were investigated through the time-resolved fluorescence anisotropy. The fluorescence anisotropy decay curves of momorcharins and it complex with NAG were described with double exponential kinetics. The longer rotational correlation times of α-momorcharin and β-momorcharin were 43.4 ns and 33.7 ns, respectively. They correspond to the correlation times of the entire rotations of momorcharins. On the other hand, the shorter rotational correlational times were referred to the rotational fluctuations of the peptide segments including Trp residue. The relationship between the entire and segmental rotations of proteins is well explained by Equations, (6) and (7) which are derived by Eq. (4).

$$r(t) = \left\{ f e^{-t/\varphi_s} + (1-f) \right\} e^{-t/\varphi_u} \tag{6}$$

$$f = \frac{\beta_s}{\beta_s + \beta_u} \tag{7}$$

Where, f is rotational freedom of Trp, φ_s and φ_u are the rotational correlation times of Trp and momorcharin itself, respectively, and β_s and β_u are the corresponding pre-exponential factor. The decay parameters in Eq. (6) and (7) were experimentally decided based on Eq. (4). The rotational freedom (f) of Trp residue was described as $f = \frac{1}{2}\cos\theta(cos\theta + 1)$ with using semi-cone-angle (θ) to show the range of the segmental rotation within the protein [28]. The fluorescence anisotropy decays of β-momorcharin and the complex with NAG were shown in Fig. 4. The decay parameters were summarized in Table 2. The longer rotational correlation times of α- and β-momorcharin were shortened and prolonged by the binding of NAG. The shortening of the rotational correlation time due to the entire rotation of α-momorcharin would be induced by the shrink of N-terminal and/or C-terminal domain because the motional freedom of Tro192 was increased about 50%. On the other hand, the motional freedom of Trp190 in β-momorcharin was suppressed from $f = 0.32$ to 0.15 corresponding to the decrease in θ from 28.5°to 18.9°. The enlargement of two terminal domains of β-momorcharin by NAG-binding which is substantiated by increasing in the longer rotational correlation time would make the movable space of Trp190 narrower.

While the shorter rotational correlation time of Trp190 was not influenced by the binding of NAG with β-momorcharin, one of Trp192 (α-momorcharin) became shorter from 0.31 ns

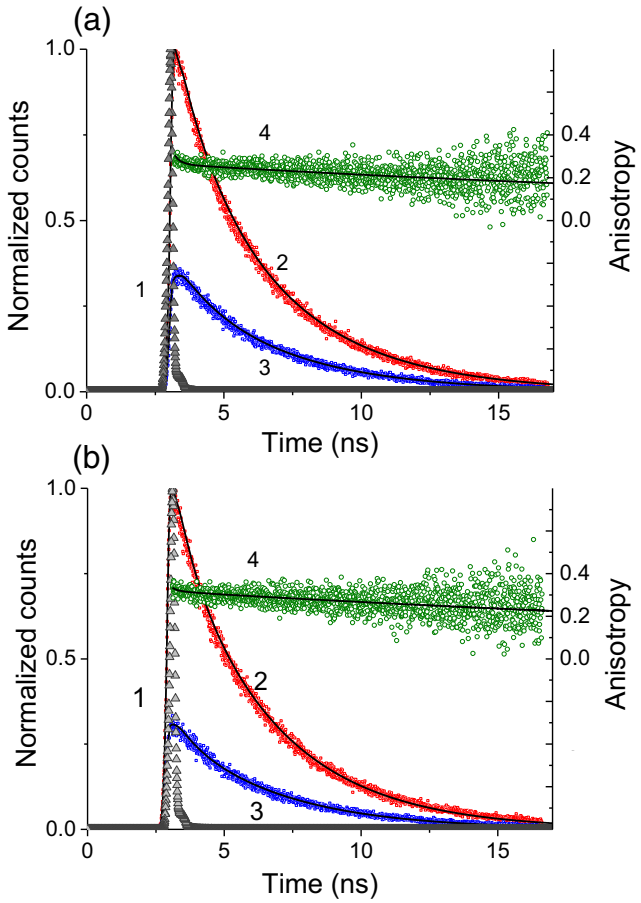

Fig. 4 The fluorescence anisotropy decays of β-momorcharin (**a**) and complex with NAG (**b**). Concentration of β-momorcharin was 0.75 μM in the 10 mM of phosphate buffer. Measurement was performed after equilibration with 30 μM of NAG in (b). Excitation wavelength, 295 nm; Emission wavelength, 350 nm; Channel width, 8.6 ps/ch. Curves 2 and 3, decays of the vertical and horizontal components against vertical excitation, respectively. The instrumental response function was indicated by spike like curve (curve 1). The fluorescence anisotropy decay (*r*) (curve 4) was calculated using the decay parameters giving the best fit to I_{VV} and I_{VH}

to 0.10 ns because of the probable liberation from the interaction with amino acid segments surrounding Trp192.

FRET between Trp and Nearest Neighboring Tyr around the Active Site

Both of two momorcharins arrange single Trp at the lid part of active site, respectively. Two Tyr residues of each momorcharin are considered to participate in the binding with substrates at the active site [13]. Therefore, it is interesting to know the distance between Tyr and Trp associating with the enzymatic activity of momorcharins. The method of Förster type of resonance excitation energy transfer (FRET) makes it possible to measure the relative distance between Tyr and Trp in proteins in aqueous solutions. Since the absorption and fluorescence spectra of Tyr distribute at higher energy side than those of Trp, the fluorescence intensity and lifetime of Tyr residue are necessary to estimate the energy transfer rate and/or efficience in the FRET studies between Tyr and Trp. However, it is difficult to measure distinctively the fluorescence of Tyr in the Trp containing protein because the fluorescence of Trp is more dominant and their fluorescences mutually overlap. But, it is possible to extract the fluorescence lifetime of Tyr by close measurements of the fluorescence decay kinetics of the acceptor, Trp. When momorcharin is excited at 285 nm, both of Trp and Tyr simultaneously reached to the excited singlet state. If the FRET from Tyr is concerned with the electronic relaxation process of Trp, the fluorescence decay kinetics of Trp is described as,

$$F(t) = \left[\frac{k_{et}D_0}{\left\{\frac{1}{\tau_A}-\frac{1}{\tau_D}\right\}}\right]\left[\exp\left(\frac{-t}{\tau_D}\right)-\exp\left(\frac{-t}{\tau_A}\right)\right] + A_0\exp\left(\frac{-t}{\tau_A}\right) \quad (8)$$

Where, k_{et} is the energy transfer rate constant, D_0 and A_0 are the coefficients associating with the concentration of the donor and acceptor molecules just after the excitation, and τ_A and τ_D are the fluorescence lifetimes of the acceptor and donor, respectively [17]. Equation (8) demonstrates that the fluorescence decay is given by sum of two components, one is

Table 2 Fluorescence anisotropy decay parameters of momorcharins (Ex:295 nm, Em:350 nm)

	$\beta 1$	$\beta 2$	$\varphi 1$ (ns)	$\varphi 2$(ns)	σ	SVR (VV)	SVR (VH)	f	θ(°)
α-MMC	0.043	0.324	0.306	43.4	1.011	1.926	1.944	0.117	16.5
α-MMC + NAG	0.072	0.334	0.101	36.2	1.030	1.947	1.914	0.177	20.5
β-MMC	0.120	0.259	0.193	33.7	1.061	1.893	1.766	0.317	28.5
β-MMC + NAG	0.056	0.314	0.187	43.4	0.996	2.070	2.165	0.151	18.9

$r(t) = \sum\beta_e\exp(-t/\varphi_i)$ $\quad f = \beta_1/\beta_1 + \beta_2$ $\quad \sqrt{(1-f)} = \frac{1}{2}\cos\theta(\cos\theta + 1)$

β: Amplitude of i-th decay componet

φ: The rotational correlation time of i-th component

f: Rotational freedom of the peptide element including Trp

θ: Cone angle when motional freedom was represented based on the cone model [15]

directly populated (the second term of Eq. (8)) and the other contributed by FRET from Tyr (the first term of Eq. (8)). The pre-exponential factor corresponding to the decay time of τ_D has to be negative when FRET from Tyr concerns in the fluorescence decay of Trp since the fluorescence lifetime of Tyr is shorter than that of Trp and furthermore the participant of k_{et} in the fluorescence decay of Tyr makes τ_D shorter. The fluorescence decay profiles of α-momorcharin excited at 285 nm were shown in Fig. 5a. Compared with the fluorescence excited at 295 nm, the decay profile excited at 285 nm showed the round form because of the rising time due to the energy transfer from Tyr residue. The fluorescence decay parameters were summarized in Table 3.

The fluorescence decay kinetics of α- and β-momorcharins were described with the triple and double exponential functions, respectively. While one of two pre-exponential factors of β-momorcharin was negatve, one of three pre-exponential factors of α-momorcharin was observed to be negative. According to Eq. (8), these results suggest that both of Trp190 of β-momorcharin and Trp192 of α-momorcharin participated in the FRET from Tyr residue. The shortest decay time of the component with the negative pre-exponential factor corresponds to the fluorescence lifetime of the energy donor. Therefore, FRET was recognized in Trp-Tyr pair of α-momorcharin. The results in Table 3 demonstrate that the lifetime of energy donor residue (Tyr) was shortened from 0.312 ns to 0.018 ns to demonstrate that the Trp-Tyr distance shrink by the binding of α-momorcharin with NAG.

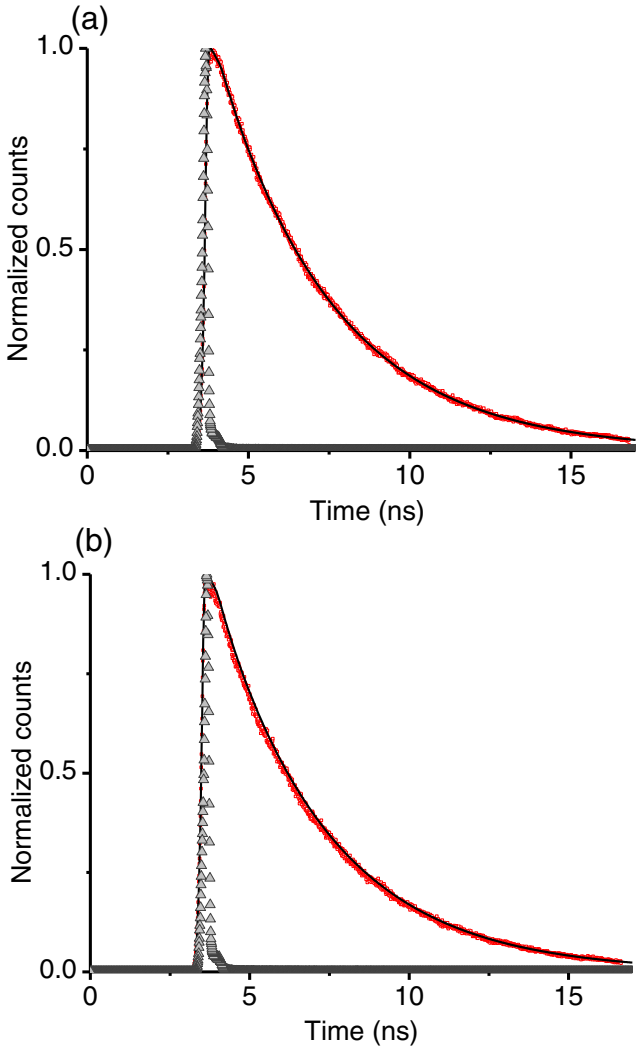

Fig. 5 The fluorescence intensity decay of α-momorcharin (**a**) and complex with NAG (**b**). The excitation and emission wavelengths were 285 and 350 nm, respectively. The instrumental response function was shown by the spike like line. The concentration of α-momorcharin was 1.59 μM and 30 μM of NAG was included in (**b**)

Generally, the rate constant of energy transfer, k_{et} is given using the lifetimes of the energy donors,

$$k_{et} = \frac{1}{\tau_D} - \frac{1}{\tau_D^0}.$$

Where, τ_D and $\tau_D{}^0$ are fluorescence lifetimes of the donor molecules in the presence and absence of FRET process. While the former was experimentally decided based on Eq. (8), the fluorescence lifetime of non-interacting tyrosine, 3.27 ns was adopted for the latter value [29]. Furthermore, k_{et} is connected with the distance (r) between the donor and acceptor though the critical distance (R_0) giving 50% of energy transfer efficiency in FRET, [30].

$$k_{et} = {}^{1}/_{\tau_D^0}\left(\frac{R_0}{r}\right)^6 \tag{9}$$

Unfortunately, R_0 of Trp-Tyr for the FRET in momorcharin would not be confirmed. But the values of R_0 for Trp-Tyr for many cases could be available. The shortest and longest R_0 are known to be 9 and 18 Å [31–34]. Using these value, our experimental results demonstrated that the distance between Trp192 and the nearest neighboring Tyr in α-momorcharin would be in the range of 6.18 Å to 12.35 Å. Since τ_D was shortened, it was clear that the corresponding distance would shrink in the complex of α-momorcharin with NAG. They were estimated to be in the range of 3.85 Å~7.71 Å. According to the X-ray structure of α-momorcharin, the disrtance between Trp192 and the nearest neighboring Tyr (Tyr70) is 9.43 Å. Although the detailed conformation of momorcharin in the aqueous solution is not necessarily same as one in the x-ray structure, our experimental FRET distance estimated from k_{et} was quite consistent with the result in the X-ray analysis. Based on the the x-ray structure of α-momorcharin, the critical distance between Tyr and Trp is 9.19 Å. When the Trp192-Tyr70 distance is calculated using this value of R_0, it is clear that Trp192 approaches about 3.55 Å to Tyr70 in α-momorcharin-NAG complex. The relative approach of Trp192 to Tyr70 near the active site was consistently shown based on the crystal structure or also using the established R_0.

Table 3 Fluorescence intensity decay parameters of momorcharins and complexes with NAG (Ex:285 nm, Em:350 nm)

	$\alpha 1$	$\alpha 2$	$\alpha 3$	τ_1(ns)	τ_{I2}(ns)	τ_{I3}(ns)	σ	SVR
α-MMC	−0.02	0.07	0.95	0.31	1.63	3.57	1.12	1.68
α-MMC + NAG	−0.19	0.09	1.09	0.02	0.40	3.50	1.06	1.80
	$\alpha 1$	$\alpha 2$		τ_{I1}(ns)	τ_{I2}(ns)		σ	SVR
β-MMC	−0.17	1.17		1.45	4.17		1.10	1.87
β-MMC + NAG	0.14	0.86		0.54	3.76		1.16	1.54

αi:The pre-exponential factor of the i-th component

τ_i:The decaytime of i-th component (ns)

σ and SVR: sigma value and serial varia nce ratio for the fitting quality

The close association of resonance excitation energy transfer with the electronic relaxation process of Trp residue is well evidenced by the negative pre-exponential factor in the fluorescence decay kinetics. The negative pre-exponential factor was recognized also in the fluorescence decay kinetics of Trp-190 in β-momorcharin and the corresponding decay time was 1.45 ns. But, no evidence indicating the FRET between Trp190 and the nearest neighboring Tyr residue in the complex of β-momorcharin with NAG was observed. The distance between Trp190 and Tyr70 was estimated to be in the range of 9.27 ~18.54 Å using the fluorescence decay time of donor residue and established R_0. However, Trp190 and Tyr70 would not be so close in mutual that FRET could be possible because the negative pre-exponential factor was not found in the fluorescence decay kinetics of Trp190 in the complex. Probably, the binding of NAG would change the conformation around the active site in β-momorcharin so that the distance between Trp190 and the nearest neighboring Tyr residue may be extended more.

NAG Binding Effects on the Enzymatic Activity

The N-glycosidase activity of momorcharin was quantitatively estimated as the quantity of released adenine from RNA per one hour (μM/h). The histogram of the enzymatic activities of α- and β-momorcharin and the NAG effects on them are shown in Fig. 6.

The enzymatic activity of α-momorcharin was reduced 25% by the binding with NAG. On the other hand, β-momorcharin is activated to 0.06 μM /h although the enzymatic activity was low in the absence of NAG. It is very interesting to recognize that such NAG effects on the N-glycosidase activity of momorcharin closely correlate with the conformation changes induced by NAG binding near the active site.

3D structure of momorcharin is consisted of N-terminal and C-terminal domains. As clearly shown in X-ray structure, the package of C-terminal domain is loose on the whole. N-terminal domain also equips loosely packed part. Therefore, it is reasonably assumed that the large conformational change by NAG binding would be caused by the shrink or swollen in the flexible parts of N- and C-terminal domains. The longer rotational correlation time of α-momorcharin was shortened from 43.4 ns to 36.2 ns by the binding of NAG. According to the well- known Einstein-Debye relationship between the rotational correlation time and molecular size of protein, this shortening of the rotational correlation time corresponds to the shrink of the volume of α-momorcharin to 80%. Gajuraj et al. and Yuan et al. reported that two molecules of NAG bound with α-momorcharin at C-terminal domain and the binding site of β-momorcharin locate at the flexible part of N-terminal domain, respectively [21, 22]. Therefore, the shrink of C-terminal domain of α-momorcharin would be a cause of the expanse of the space between the N- and C-terminal domain to enlarge the motional freedom of peptide element including Trp residue ($f = 0.12$ to $f = 0.18$) as shown in Fig. 7.

Such conformational change reduced 25% the enzyme activity of α-momorcharin. On the other hand, the longer rotational correlational time was prolonged from $\phi_2 =$ 33.7 ns to $\phi_2 = 43.0$ ns and the enzymatic activity of β-momorcharin was simultaneously 2 times enhanced by the binding of NAG. The enlargement of N-terminal domains

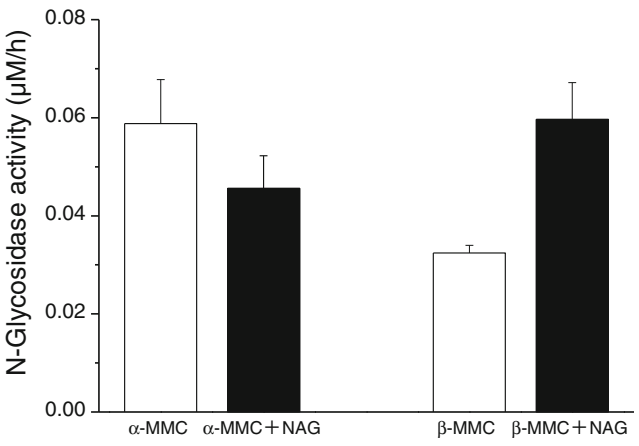

Fig. 6 NAG effects on the enzymatic activity of momorcharins. The concentration of α-momorcharin and β-momorcharin were 0.75 μM. Concentration of RNA was 40 μg/mL. The concentration of NAG was 2 mM

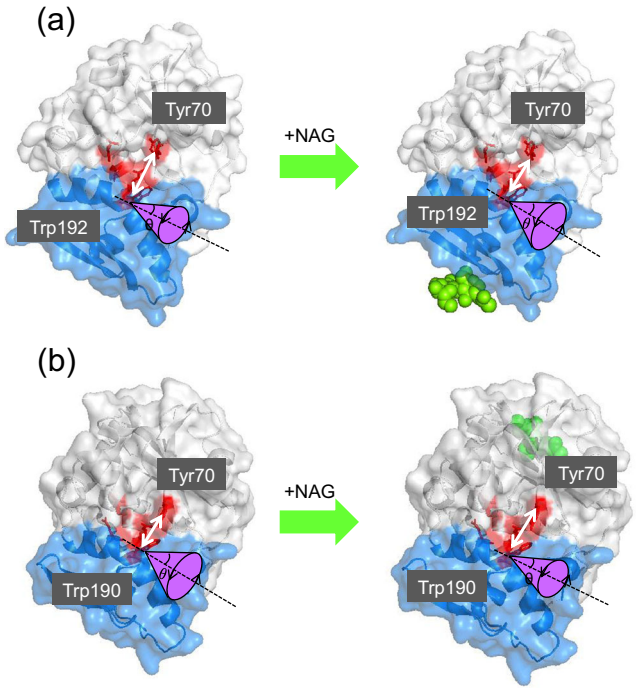

Fig. 7 The schematic representations of the structural changes near the active site of momorcharins induced by the bindings of NAG. NAG shown by small balls. **a** α-momorcharin: C-terminal domain is shrunk to increase approaching to Tyr-70 and motional freedom of Trp-192 by binding with flexible C-terminal domain. **b** β-momorcharin: The binding of NAG with N-terminal domain causes the expansion of N-terminal domain to extend the distance between Trp190 and Tyr70 and to reduce the motional freedom of Trp190. Two binding molecules of NAG locate behind the N-terminal domain

by NAG-binding reduced the freedom of rotational motion of Trp from $f = 0.32$ to $f = 0.15$. Such correlation between the rotational freedom of Trp residue and N-glycosidase activity of momorcharins suggests that the shrink of C-terminal domain of α-momorcharin and expansion of N-terminal domain of β-momorcharin caused by NAG binding must regulate the approach of substrate and release of product at the active site of momorcharins.

Another conformation change near the active site close correlate with the enzyme activity was shown in the distance between Trp-192 and Tyr-70 of α-momorcharin. FRET analysis in the present studies demonstrated that Trp192-Tyr 70 distance was shortened about 3.5–3.6 Å concomitantly with the shrink of C-terminal domains. On the other hand, the distance Trp190 and nearest neighboring Tyr of β-momorcharin was extended by the NAG binding. Although we cannot form a definite conclusion since X-ray structure of β-momorcharin is not confirmed yet, the distance between Trp and nearest neighboring of Tyr deeply participates in the N-glycosidase activity of momorcharin. The approach of Trp which locate lid part of active center to the substrate binding Tyr residues suppresses and contrarily the separation promotes the enzyme activity.

Conclusion

It was confirmed that two types of Type I RIPs, α- and β-momorcharin retained strong affinity to NAG. Hitherto, it have been considered that NAG binding gave no effect on the enzymatic activity of momorcharin since it bind at the flexible part of N-terminal domain or C-terminal domain of momorcharin apart far from the active center. However, the enzymatic activities of α- and β-momorcharin were suppressed and accelerated by the binding with NAG, respectively. The time-resolved fluorescence anisotropy and FRET analysis of single Trp which located at the lid part of active center described well the essential conformational changes for the regulation of enzymatic activity of momorcharins. As shown in Fig. 7, in response to changes in the enzymatic activity, the packing and domain size of α-momorcharin shrank to extend the lid part of the active center and to access Trp residue to the neighboring Tyr. On the other hand, the movable space of Trp was limited and the distance between Trp and Tyr were extended near the active site in the case of β-momorcharin.

References

1. Andrea B, Massimo B, Stefania M, Maria GB, Letizia P (2016) Ribosome-inactivating proteins from plants: a historical overview. Molecules 21:1627–1646
2. Au TK, Collins RA, Lam TL, Ng TB, Fong WP, Wan DCC (2000) The plant ribosome inactivating proteins luffin and saporin are potent inhibitors of HIV-1 integrase. FEBS Lett 471:169–172
3. Wang YX, Jacob J, Wingfield PT, Palmer I, Stahl SJ, Kaufman JD, Huang PL, Huang PL, Lee-Huang S, Torchia DA (2000) Anti-HIV and anti-tumor protein MAP30, a 30 kDa single-strand type-I RIP, shares similar secondary structure and β-sheet topology with the a chain of ricin, a type-II RIP. Protein Sci 9:138–144
4. Corrado G, Bovi PD, Ciliento R, Gaudio L, Maro AD, Aceto S, Lorito M, Rao R (2005) Inducible expression of a Phytolacca heterotepala ribosome-inactivating protein leads to enhanced resistance against major fungal pathogens in tobacco. Phytopathology 95:206–215
5. Park S-W, Stevens NM, Vivanco JM (2002) Enzymatic specificity of three ribosome-inactivating proteins against fungal ribosomes, and correlation with antifungal activity. Planta 216:227–234
6. Endo Y, Mitsui K, Motizuki K, Tsurugi K (1987) The mechanism of action of ricin and related toxic lectins on eukaryotic ribosome. The site and the characteristic of the modification in 28S ribosomal RNA caused by the toxins. J Biol Chem 262:5908–5912
7. Barbieri L, Gorini P, Valbonesi P, Castiglioni P, Stirpe F (1994) Unexpected activity of saparins. Nature 372:624
8. Barbieri L, Valbonesi P, Bonora E, Gorini P, Bolognesi A, Stirpe F (1997) Polynucleotide:adenosine glycosidase activity of ribosome-inactivating proteins: effect on DNA, RNA and ploy(a). Nucleic Acids Res 25:518–522
9. Mock JWY, Ng TB, Wong RNS, Yao QZ, Yeung HW, Fong WP (1996) Demonstration of ribonuclease activity in the plant

ribosome-inactivating proteins alpha- and beta-momorcharins. Life Sci 59:1853–1859
10. Carnicelli D, Brigotti M, Alvergna P, Pallanca A, Sperti S, Montanaro L (1997) Cofactor requirement of ribosome-inactivating proteins from plants. J Exp Bot 48:1519–1523
11. Brigotti M, Carnicelli D, Alvergna P, Pallanca A, Sperti S, Montanaro L (1995) Differential up-regulation by tRNAs of ribosome-inactivating proteins. FEBS Lett 373:115–118
12. Brigotti M, Keith G, Pallanca A, Carnicelli D, Alvergna P, Dirheimer G, Montanaro L, Sperti S (1998) Identification of the tRNA with up-regulates agrostin, barley RIP and PAP-S, three ribosome-inactivating proteins of plant origin. FEBS Lett 431: 259–262
13. Ren J, Wang Y, Dong Y, Stuart ID (1994) The N-glycosidase mechanism of ribosome-inactivating proteins implied by crystal structures of α-momorcharin. Structure 2:7–16
14. Lakowicz, J.R. (2006) Principles of fluorescence spectroscopy. Third Edition. Springer. pp 529–576
15. Flanklyn GP (1991) Time-resolved fluorescence techniques: methods and applications in biology. Curr Opin Struct Biol 1: 1054–1059
16. Eisinger J, Feuer B, Lamola AA (1969) Intramolecular singlet excitation transfer. Applications to polypeptides. Biochemistry 8: 3908–3914
17. Fukunaga Y, Nishimoto E, Yamashita K, Otosu T, Yamashita S (2007) The partially unfold state of β-momorcharin characterized with steady-state and time-resolved fluorescence studies. J Biochem 141:9–18
18. Fukunaga Y, Nishimoto E, Otosu T, Murakami Y, Yamashita S (2008) The unfolding of α-momorcharin proceeds through the compact folded intermediate. J Biochem 144:457–466
19. Fukunaga, Y. (2007) Steady-state and Time-resolved fluorescence studies on structure, dynamics, function and stability of ribosome-inactivating proteins. Doctoral Dissertation, Graduate school of Kyushu University
20. Stripe F, Battelli MG (2006) Ribosome-inactivating proteins: progress and problems. Cell Mol Life Sci 63:1850–1866
21. Gajraj SK, Nisha P, Mau S, Baskar S, Punit K, Sujata S, Tej PS (2012) Crystal structures of a type-1 ribosome inactivating protein from Momordica balsamina in the bound and unbound states. Biophys. Acta 1824:679–691
22. Yuan YR, He YN, Xiong JP, Xia ZX (1999) Three-dimensional structure of β-momorcharin at 2.55 Å resolution. Acta Crystallogr Sect D 55:1144–1151
23. Nakashima H, Fukunaga Y, Ueno R, Nishimoto E (2014) Sugar biding effects on the enzymatic reaction and conformation near the active site of pokeweed antiviral protein revealed by fluorescence spectroscopy. J Fluoresc. 24:951–958
24. Yao M, Sen L, Shuangfeng L, Xiang F, Guangrui L, Yanfa M (2014) A novel method for simultaneous production of two ribosome-inactivating proteins, a-MMC and MAP30 from *Momordica charantia L*. PLoS One 9:e101998
25. Fong WP, Poon YT, Wong TM, Mock JWY, Ng TB, Wong RNS, Yao QZ, Yeung HW (1996) A highly efficient procedure for purifying the ribosome-inactivating proteins α- and β-momorcharins from Momordica charantia seeds, N-terminal sequence comparison and establishment of their N-glycosidase activity. Life Sci 59:901–909
26. Nishimoto E, Yamashita S, Szabo AG, Imoto T (1998) Internal motion of lysozyme studied by time-resolved fluorescence depolarization of tryptophan residues. Biochemistry 37:5599–5607
27. Mckinon AE, Szabo AG, Miller DR (1977) The deconvolution of photoluminescence data. J Phys Chem 81:1564–1570
28. Lipari G, Szabo A (1982) Model-free approach to the interpretation of nuclear magnetic resonance relaxation in macromolecules. 2. Analysis of experimental results. J Am Chem Soc 104:4559–4570
29. Ross, J.B.A., Laws, W.R., Rousslong, K.W., and Wyssbrod, H.R., (1992) Tyrosine fluorescence and phosphorescence from proteins and polypeptide. In topics in fluorescence spectroscopy (Lakowicz, J.R., ed.) Biochemical applications, plenum Press, New York, Vol 3. pp 1–63
30. Lakowicz, J.R. (2006) Principles of fluorescence spectroscopy. Third Edition. Springer, pp 443–475
31. Weber G (1960) Fluorescence-polarization spectrum and electronic-energy transfer in tyrosine, tryptophan and related compounds. Biochem J 75:335–345
32. Eisinger J (1969) Intramolecular energy transfer in adenocorticotropin. Biochemistry 8:3902–3908
33. Moreno MJ, Prieto M (1993) Interaction of the peptide hormone adenocorticotropin, ACTH(1-24), with a membrane model system: a fluorescence study. Photochem Photobiol 57(3):431–437
34. Pearce SF, Hawrot E (1990) Intrinsic fluorescence of binding-site fragments of the nicotinic acetylcholine receptor: perturbations produced upon binding α-bungarotoxin. Biochemistry 29:10649–10659